Electronic Supplementary Material (ESI) for Environmental Science: Processes & Impacts.

Investigation of perfluoroalkyl substances in proglacial rivers and permafrost seep in a High Arctic watershed

Electronic Supplementary Information

John MacInnis[a*], Amila O. De Silva[b*], Igor Lehnherr[c], Derek C.G. Muir[b], Kyra A. St. Pierre[d], Vincent L. St. Louis[e], and Christine Spencer[b]

[a]Department of Chemistry, Memorial University, St. John's, NL A1B 3X7

[b]Aquatic Contaminants Research Division, Environment and Climate Change Canada
Burlington, ON L7S 1A1

[c]Department of Geography, Geomatics and Environment, University of Toronto, Mississauga, ON L5L 1C6

[d]Institute for the Oceans and Fisheries, University of British Columbia, Vancouver, BC V6T 1Z4

[e]Department of Biological Sciences, University of Alberta, Edmonton, AB T6G 2E9

***Corresponding Authors**

john.macinnis@mun.ca

amila.desilva@canada.ca

Tables: 9

Figures: 7

Pages: 26

Table of Contents

Tables

Figures

Section S1. Permafrost dynamics in Arctic soils. Subsurface Arctic soils are categorized into two zones. The first zone is known as the active layer, the top layer of soil that undergoes seasonal freeze-thaw cycles.[1] The active layer is underlain by a second zone, permafrost, which is ground (i.e., soil) that has maintained a temperature of 0 °C for at least two consecutive years.[1] During the Arctic summer, soils in the active layer thaw and the ice contained within those soils melts. Precipitation from the atmosphere and snowmelt from the Arctic landscape can infiltrate surface soils and add to the meltwater reservoir in the active layer (Figure S1).[1] Water can be retained within the active layer or discharged to the surface (e.g., via seeps). During the fall, when temperatures decrease, water retained in the active layer will refreeze until the following summer. These dynamics change under the influence of climate warming. For example, warmer temperatures can promote active layer deepening, a process where higher temperatures enhance the thawing of soils at depth (Figure S1).[1] An important consequence of active layer deepening is that permafrost soils, which were once perennially frozen, thaw, and the ice contained within those soils melts and can become integrated in the active layer.[1] Climate warming-induced active layer deepening is a mechanism that can account for the remobilization of historically archived contaminants in ice contained in permafrost soils to freshwater ecosystems in the Arctic.

Section S2. Study area. The Lake Hazen catchment is sheltered from polar winds on the northwest by the Garfield Mountain Range. Glaciers cover ~41% of the Lake Hazen watershed (7156 km^2), and their areas range between 6 to 1041 km^2 (Table S1). The delivery of meltwaters and sediments by glacial fed rivers into Lake Hazen promotes water column mixing via dense and turbid underflows.[2] Annual glacial runoff in the Lake Hazen watershed in 2015 is dominated by inputs from the Henrietta Nesmith River (0.291 km^3, 30%), Gilman River (0.192 km^3, 20%), Very River (0.165 km^3, 17%), Turnabout River (0.082 km^3, 8%), Abbé River (0.061 km^3, 6%), and Snowgoose River (0.026 km^3, 3%). Lake Hazen is drained by the Ruggles River into Chandler Fiord.[2] The annual output by the Ruggles River was 1.093 km^3 in 2015.[2] Further information on rivers in the Lake Hazen watershed is presented in Table S1.

Skeleton Lake (1.9 ha, max. depth = 4.7 m, 299 m above sea level) drains into two small downstream ponds (<1 ha, < 2.5 m deep), and a riparian and meadow wetland before draining into Skeleton Creek. The riparian wetland along the Skeleton Continuum is surrounded by vegetation including alpine foxtail (*Alopecurus alpinus*), arctic willow (*Salix arctica*), cotton grass (*Eriophorum spp*.), two-flowered rush (*Juncus biglumis*), and water sedge (*Carex aquatilis*).[3] The shallow meadow wetland along the Skeleton Continuum is characterized by a relatively homogeneous cover of water sedge, cotton grass, bryophytes, and graminoids.[4] Skeleton Creek provides a summer habitat for juvenile Arctic char (*Salvelinus alpinus*).[5]

Local contamination arising from anthropogenic activity at the Lake Hazen base camp, which has been in operation since 1957 and is within approximately 2 km of the continuum, should be considered as a potential source of PFAS, including emissions from weatherproofed gear (e.g., garments and tents), waste incineration, and aircraft activity. However, PFAS concentrations at sites closest to the camp (i.e., S4 and S5) were generally not elevated relative to other sites along the continuum. The presence of PFECHS along the Skeleton Continuum, however, may be attributed to aircraft activity, considering its reported use as an additive in aircraft hydraulic fluids.[6] In a survey of water, biota, and sediment in lakes on Cornwallis Island, PFECHS was only detected in those lakes that were near the Resolute airport and not in the more remote lakes.[7] Whether PFECHS occurs in background sites in the Arctic is less clear, with one study reporting PFECHS deposition up to 4 ng m^{-2} $year^{-1}$ in the Devon Ice Cap[8] and a follow-up study reporting PFECHS as <LOD in the same area.[9] Should the Skeleton Continuum receive additional PFAS inputs from the base camp, then these would be magnified due to low flow. Historical emissions from aircraft and products may also be distributed during the landscape disturbance from aircraft landing and taking off. As such, while the frequency of aircraft activity is low within this region, we recognize the possibility of the spatial pattern of PFAS in the Lake Hazen continuum being influenced by this type of landscape perturbation.

While local sources are possible, long-range atmospheric transport is expected to be the primary pathway for PFAS to the Lake Hazen watershed. In an earlier study, we hypothesized that the presence of PFCA in Lake Hazen snowpacks in 2013 and 2014 was attributed to the long-range atmospheric transport and oxidation of fluorotelomer alcohols, pursuant to even-odd PFCA congener ratios in snowpacks.[10] In another study, we found that PFOA, PFDA, and PFBS fluxes in a Lake Hazen sediment core correlated with fluorotelomer production volumes during 1963-2005.[11] These observations highlight that long-range atmospheric transport is an important mechanism, accounting for contemporary and historically archived PFAS in the Lake Hazen watershed.

Section S3. Chemicals. PFAS analyzed in this study are: perfluorobutanoic acid (PFBA), perfluoropentanoic acid (PFPeA), perfluorohexanoic acid (PFHxA), perfluoroheptanoic acid (PFHpA), perfluorooctanoic acid (PFOA), perfluorononanoic acid (PFNA), perfluorodecanoic acid (PFDA), perfluoroundecanoic acid (PFUnDA), perfluorododecanoic acid (PFDoDA), perfluorotridecanoic acid (PFTrDA), perfluorotetradecanoic acid (PFTeDA), perfluorohexadecanoic acid (PFHxDA), perfluorobutane sulfonic acid (PFBS), perfluorohexane sulfonic acid (PFHxS), perfluoroheptane sulfonic acid (PFHpS), perfluorooctane sulfonic acid (PFOS), perfluoro-4-ethyl-cyclohexane sulfonic acid (PFECHS), perfluorodecane sulfonic acid (PFDS), and perfluorooctane sulfonamide (FOSA). PFAS standards (native and isotopically-labeled) were purchased from Wellington Laboratories (Guelph, Ontario) and Chiron AS (Trondheim, Norway). The PFECHS standard used in this study is composed of cis/trans isomers and other minor impurities such as perfluoro-4,4-dimethylcyclohexane sulfonate, perfluoro-3-ethyl-3-methylcyclopentane sulfonate, and perfluoro-3-propylcyclopentane sulfonate. PFECHS was quantified in samples by integrating all peaks (i.e., cis/trans isomers and impurities) across their retention time window. Methanol and water (Optima™ Grade) were purchased from Fisher Scientific (New Hampshire, USA), glacial acetic acid (ACS Grade) was purchased from EMD (Etobicoke, Ontario), ammonium acetate (>98%) was purchased from Sigma Aldrich (Missouri, USA), and ammonia (Suprapur® 25 %) was purchased from Merck (New Jersey, USA).

Section S4. QA/QC. PFAS were quantified using a 15 point calibration curve. Before laboratory analysis, water samples were spiked with 30 µL of an internal standard (IS) mixture (Table S2) and concentrated using an Oasis® weak anion exchange solid phase extraction (WAX-SPE, cartridge: 6 cm^3, 150 mg, 30 µm). Accuracy was evaluated by spiking 30 µL of a native PFAS standard mixture (35 ng mL^{-1}) into water samples (Tables S2 and S3). These samples were analyzed concurrently with other Lake Hazen water samples. The analytical laboratory annually participates in the Northern Contaminants Program Interlaboratory Evaluation and has consistently achieved high performance for accuracy based on low z-scores obtained from interlaboratory trials. The recovery of PFAS in samples was calculated by comparing analyte peak area in sample extracts to analyte peak area in a solvent standard at equivalent concentrations (Table S3). Likewise, matrix effects were evaluated by comparing the peak area of an instrument performance (IP) PFAS standard added post-extraction to those in a solvent standard at equivalent concentrations. Extraction blanks were used to evaluate positive biases during the laboratory analysis. This consisted of extracting a WAX-SPE cartridge spiked with 30 µL of a PFAS IS mixture (4 ng mL^{-1}, Tables S2 and S3). Field blanks were collected to evaluate biases from sampling and transport. Field blank collection was conducted by transporting 500 mL of high-performance liquid chromatography (HPLC)-grade water to the Lake Hazen region, and exposing these samples to the atmosphere for ten seconds. PFAS concentrations in field blanks were similar to those in HPLC-grade water from the laboratory (i.e., stay blank), indicating sampling and transportation are not sources of contamination (Table S3). PFAS concentrations in samples were method blank, recovery, and matrix corrected.

Section S5. Estimating mass transfer of PFAS into the Lake Hazen watershed using the LOADEST model. We evaluated inputs by glacial rivers and snowmelt compared to the output via the Ruggles River outflow to estimate the net mass transfer of PFAS in the lake watershed. The major glacial rivers and their corresponding annual runoff (2015-2016) included in this estimation were Henrietta-Nesmith River (0.183 km^3 $year^{-1}$), Very River (0.122 km^3 $year^{-1}$), Gilman River (0.118 km^3 $year^{-1}$), Turnabout River (0.053 km^3 $year^{-1}$), Abbé River (0.038 km^3 $year^{-1}$), and Snowgoose River (0.016 km^3 $year^{-1}$), as previously reported.[2] To provide a first-order estimate of glacial river fluxes, PFAS concentrations were related to discharge volume by log-linear models using the rLOADEST package in R.[12] While we fully acknowledge that a relatively small number of points were used to generate PFAS flux estimates, the model R^2, bias percentage, partial ratio and Nash Sutcliffe efficiency index suggested good fits between the concentration and discharge data (see Table S6).

Section S6. Seasonal water column profiles in Skeleton Lake. Although the water retention time is not known for Skeleton Lake (S2), the water column profile during the ice-covered period in May 2013 was likely representative of integrated hydrological inputs that were delivered to the lake prior to (e.g., snowmelt from 2011) and during summer 2012, because the surface of S2 freezes over beginning in September, preserving hydrological inputs under the ice until the following spring. The water column profile during the ice-free period in July 2015 was likely representative of integrated hydrological inputs that were delivered to the lake prior to and during summer 2015.

Several PFAS were detected at 1.5 and 3 m depths in S2 during the ice-covered period in 2013, including C_6-C_{10} PFCA and PFBS, whereas PFUnDA, PFOS, and FOSA were only detected at 1.5 m (Figure S6). The latter congener profile shares some similarities with those during the ice-free period (Table S8), although PFBA, PFTrDA, PFECHS, and PFHpS were only detected in S2 during 2015. PFHxA was most abundant in the ice-covered water column (0.70-0.42 ng L^{-1}), accounting for 44-52% of the ΣPFAS concentration (0.94-1.3 ng L^{-1}), while PFBA was most abundant in the ice-free water column (median 3.1 ng L^{-1}), accounting for 76-81% of ΣPFAS concentrations (3.6-4.7 ng L^{-1}). All PFAS congener concentrations in S2 at 1.5 m were higher than those at 3 m during the ice-covered period. We acknowledge that elevated PFAS concentrations at 1.5 m could be due to snowmelt percolating through cracks in the lake ice, as observed previously in the Lake Hazen water column.[10] Although, PFBA was not detected in the water column of S2 during the ice-covered period, which would be an expected outcome, as it was detected in Lake Hazen snowpacks in 2013.[10] We have also considered the likelihood of cryoconcentration, where PFAS are enriched in waters beneath the lake ice surface after being excluded during freezing. This could provide a rationale for higher PFAS congener concentrations during the ice-covered period in comparison to the ice-free period. For example, PFHxA and PFDA concentrations were approximately 2 to 4-times higher than those measured during the ice-free period (Figure S6). However, the concentration of some PFAS congeners (e.g., PFOA, PFBS) were similar in both water columns (Figure S6). Thus, it is difficult to confirm this effect, because S2 was influenced by different melting inputs during each period, based on the observed differences in congener profiles and concentrations.

The absence of PFBA in the ice-covered water column is interesting because it has been commonly measured as a dominant congener in most samples from the Lake Hazen watershed (Tables S5 and S8). The reason for the absence of PFBA in the ice-covered water column of S2 is not clear since other measurements were not made in or around the lake (e.g., ice-free summer water column and snowpacks in 2012). However, if PFBA was delivered to S2 in 2012, then it is unlikely that sediments in the lake would be a long-term sink for PFBA, considering it has not been previously measured in Lake Hazen sediments.[11] Furthermore, PFBA is expected to exist as a deprotonated, anion ($pK_a \sim 0$)[13] under environmental conditions representative of the aqueous environment, imparting high water solubility. Despite these uncertainties, these data nevertheless provide insights into the hydrological inputs of PFAS to S2 during ice-covered and ice-free periods in 2013 and 2015, respectively.

Table S1. Overview of rivers in the Lake Hazen watershed.[2] Discharge data are shown as the mean ± standard error estimated daily from 1 July to 15 August 2015. *The Blister River watershed could not be delineated due to low resolution of the Canadian Digitial Elevation Model, and its glacier area is estimated according to the Randolph Glacier Inventory, as described in St. Pierre et al.[2]

River	Glacier Area (km^2)	Watershed Area (km^2)	Length (km)	Discharge ($m^3\ s^{-1}$)
Henrietta Nesmith River	1041	1274	4.3	76 ± 16
Gilman River	708	992	21.2	51 ± 12
Very River	269	1035	42.5	43 ± 6.0
Turnabout River	259	678	55.3	23 ± 4.8
Abbé River	204	390	20.9	17 ± 3.6
Snowgoose River	87	222	15.6	17 ± 3.6
Blister River*	6	N/A	11.2	N/A

Table S2. Overview of PFAS standards and tandem mass spectrometry parameters. Precursor-product ion mass-to-charge ratios (m/z) in bold text are used for PFAS quantitation and qualifier m/z in normal text are used for confirmation.

Native		IS		IP	
PFBA	**213 > 169**	$^{13}C_4$ PFBA	**217 > 172**	$^{13}C_3$ PFBA	**216 > 172**
PFPeA	263 > 219	$^{13}C_5$ PFPeA	**268 > 223**	$^{13}C_3$ PFPeA	**266 > 222**
PFHxA	**313 > 269** 313 > 119	$^{13}C_2$ PFHxA	**315 > 270**	$^{13}C_5$ PFHxA	**318 > 273**
PFHpA	**363 > 319** 363 > 119	$^{13}C_4$ PFHpA	**367 > 322**		
PFOA	**413 > 369** 413 > 169	$^{13}C_4$ PFOA	**417 > 372**	$^{13}C_2$ PFOA	**415 > 370**
PFNA	**463 > 419** 463 > 219	$^{13}C_5$ PFNA	**468 > 423**	$^{13}C_9$ PFNA	**472 > 427**
PFDA	**513 > 469** 513 > 219	$^{13}C_2$ PFDA	**515 > 470**	$^{13}C_6$ PFDA	**519 > 474**
PFUnDA	**563 > 519** 563 > 269	$^{13}C_2$ PFUnDA	**565 > 520**	$^{13}C_7$ PFUnDA	**570 > 525**
PFDoDA	**613 > 569** 613 > 169	$^{13}C_2$ PFDoDA	**615 > 570**		
PFTrDA	**663 > 619** 663 > 169	$^{13}C_2$ PFDoDA	**615 > 570**		
PFTeDA	**713 > 669** 713 > 169	$^{13}C_2$ PFTeDA	**715 > 670**		
PFHxDA	**813 > 769** 813 > 169	$^{13}C_2$ PFHxDA	**815 > 770**		
PFBS	**299 > 99** 299 > 80	$^{13}C_3$ PFBS	**302 > 99**		
PFHxS	**399 > 99** 399 > 80	$^{18}O_2$ PFHxS	**403 > 103**	$^{13}C_3$ PFHxS	**402 > 99**
PFHpS	**449 > 99** 449 > 80	$^{13}C_4$ PFOS	**503 > 99**		
PFOS	**499 > 99** 499 > 80	$^{13}C_4$ PFOS	**503 > 99**	$^{13}C_8$ PFOS	**507 > 99**
PFDS	**599 > 99** 599 > 80	$^{13}C_4$ PFOS	**503 > 99**		
PFECHS	**461 > 99** 461 > 381	$^{18}O_2$ PFHxS	**403 > 103**		
FOSA	**498 > 78**	$^{13}C_8$ FOSA	**506 > 78**		

Table S3. The limits of detection (LOD) and quantification (LOQ), PFAS concentrations in blanks, and recoveries of PFAS internal (IS), instrument performance (IP), and native standards in water samples. Concentrations and uncertainties are expressed as ng L^{-1} and standard error, respectively.

	(ng L^{-1})		**Blanks (ng L^{-1})**		**Recovery (%)**		
PFAS	**LOD**	**LOQ**	**Field**	**Stay**	**IS**	**IP**	**Native**
PFBA	0.010	0.040	<0.010-1.2	0.019	79±5	101±6	101
PFPeA	0.010	0.050	<0.010	<0.010	89±4	117±4	105
PFHxA	0.005	0.020	0.011-0.059	<0.005	87±3	107±3	97
PFHpA	0.002	0.007	<0.002-0.019	<0.002	94±2		98
PFOA	0.003	0.010	0.014-0.031	0.0077	105±1	127±2	98
PFNA	0.002	0.008	<0.002	<0.002	96±1	118±1	101
PFDA	0.003	0.010	<0.003-0.030	<0.003	90±2	119±1	97
PFUnDA	0.003	0.009	<0.003	<0.003	86±1	124±1	96
PFDoDA	0.002	0.007	<0.002	<0.002	67±1		95
PFTrDA	0.002	0.006	<0.002	<0.002			58
PFTeDA	0.003	0.010	<0.003	<0.003	30±1		91
PFHxDA	0.010	0.040	<0.010	<0.010	75±4		90
PFBS	0.002	0.006	<0.002	<0.002	91±2		87
PFHxS	0.0007	0.002	<0.0007	<0.0007	95±1	115±1	88
PFHpS	0.0009	0.003	<0.0009	<0.0009			93
PFOS	0.001	0.003	<0.001	<0.001	90±3	118±1	95
PFECHS	0.001	0.003	<0.001	<0.001			93
PFDS	0.0006	0.002	<0.0006	<0.0006			77
FOSA	0.0002	0.0007	<0.0002	<0.0002	14±2		101

Table S4. Overview of liquid chromatograph gradient elution, mass spectrometric, and inlet parameters.

Liquid Chromatograph Gradient Elution				**Mass Spectrometer/Inlet**	
Time (min)	**Flow Rate (mL min^{-1})**	**H_2O (%)**	**MeOH (%)**	Ionization mode: electrospray negative	
0	0.400	75	25		
0.5	0.400	75	25	Capillary Voltage (kV)	0.6
5.0	0.400	15	85	Source Temperature (°C)	150
5.1	0.400	0	100	Desolvation Gas Temperature (°C)	450
5.6	0.400	0	100	Cone Gas Flow (L hr^{-1})	150
7.0	0.550	0	100	Desolvation Gas Flow (L hr^{-1})	800
9.0	0.400	75	25	Collision Gas Flow (mL min^{-1})	0.15
13.0	0.400	75	25	Nebulizer Pressure (bar)	7
Inlet parameters					
Column Temperature (°C)	50				
Injection Volume (μL)	9				

Table S5. Concentration ranges (ng L^{-1}) and detection frequencies (%) in the Lake Hazen area during June 2012 (Blister and Snowgoose Rivers), May 2014 (Blister and Snowgoose Rivers and Skeleton Creek), and July 2015 (Blister, Snowgoose, Henrietta Nesmith, Abbé, Turnabout, and Very Rivers). Lake Hazen water column data is shown for the ice-free period in 2015 (0-250 m depths).[10] Other Arctic sites are shown for comparison. Detection frequencies (bolded in parentheses) are calculated as the percent number of samples out of the sample size with concentrations >LOD. Notes: N.M = not measured; surface runoff from Longyearbyen[15] is impacted by fire-fighting activities; water column depths[14] in Lake A are 2, 10, and 32 m; and concentrations reported by Kwok et al.[16] are shown as means.

Area	**Lake Hazen (82° N)**					**Lake A (83° N)**	**Lake Linnévatnet (78° N)**	**Ny-Ålesund (79° N)**	**Longyearbyen (78° N)**	
Type	**Rivers and Creeks**			**Ruggles River Outflow**	**Water Column[10]**	**Water Column[14]**	**Surface Water[15]**	**Runoff Meltwater[15]**	**Surface Runoff[15]**	**River Water[16]**
Sample Size	**2**	**10**	**12**	**1**	**15**	**6**	**20**	**7**	**3**	**6**
Year	**2012**	**2014**	**2015**	**2015**	**2015**	**2008**	**2015**	**2016**	**2015**	**2006**
PFBA	5.2-6.2 **(100)**	1.1-12 **(100)**	0.62-3.3 **(100)**	0.44	<0.01-0.15 **(93)**	N.M	<0.08-1.37 **(65)**	2.0-9.1 **(100)**	<0.08 **(0)**	1.2
PFPeA	<0.010-0.64 **(50)**	<0.010-1.2 **(80)**	<0.010-0.098 **(67)**	<0.010	<0.010 **(0)**	N.M	<0.01 **(0)**	<0.01 **(0)**	3.07-3.86 **(100)**	1.0
PFHxA	0.45-0.60 **(100)**	0.11-1.9 **(100)**	0.050-0.20 **(100)**	0.016	0.009-0.019 **(100)**	N.M	<0.02-0.13 **(20)**	<0.03 **(0)**	14.8-16.5 **(100)**	0.26
PFHpA	0.66-0.69 **(100)**	0.096-2.7 **(100)**	0.044-0.28 **(100)**	0.026	0.017-0.030 **(100)**	<0.0002-0.105	<0.03-0.42 **(70)**	<0.03 **(0)**	4.07-4.48 **(100)**	0.15
PFOA	0.85-1.0 **(100)**	0.098-2.9 **(100)**	0.10-0.33 **(100)**	0.066	0.027-0.058 **(100)**	0.009-0.125	<0.06-1.78 **(85)**	<0.03 **(0)**	5.35-5.62 **(100)**	0.30
PFNA	0.30-0.47 **(100)**	0.025-0.97 **(100)**	0.037-0.26 **(100)**	0.026	0.014-0.089 **(100)**	0.006-0.143	<0.03-0.16 **(65)**	<0.02 **(0)**	0.85-0.87 **(100)**	0.10
PFDA	0.053-0.075 **(100)**	<0.003-0.12 **(90)**	<0.003-0.11 **(58)**	<0.003	<0.003 **(0)**	0.004-0.026	<0.02-0.61 **(80)**	<0.008 **(0)**	<0.008 **(0)**	0.019
PFUnDA	<0.003-0.018 **(50)**	<0.003-0.006 **(20)**	<0.003-0.009 **(17)**	<0.003	<0.003-0.031 **(13)**	0.0014-0.011	<0.12 **(0)**	<0.009 **(0)**	<0.009 **(0)**	0.011
PFDoDA	<0.002 **(0)**	<0.002-0.018 **(10)**	<0.002 **(0)**	<0.002	<0.002 **(0)**	<0.0036	<0.02-0.16 **(75)**	<0.005 **(0)**	<0.005 **(0)**	0.0076
PFTrDA	<0.002 **(0)**	<0.002-0.016 **(10)**	<0.002 **(0)**	<0.002	<0.002 **(0)**	N.M	<LOQ **(0)**	<LOQ **(0)**	<LOQ **(0)**	N.M
PFTeDA	<0.003 **(0)**	<0.003-0.005 **(10)**	<0.003 **(0)**	<0.003	<0.003 **(0)**	N.M	N.M	N.M	N.M	<0.005
PFBS	0.18-0.32 **(100)**	0.034-0.15 **(100)**	<0.002-0.053 **(75)**	<0.002	<0.002 **(0)**	<0.0009-0.017	<0.025 **(0)**	<0.003 **(0)**	2.33-2.41 **(100)**	<0.025
PFHxS	0.050-0.068 **(100)**	0.004-0.034 **(100)**	<0.0007 **(0)**	<0.0007	<0.0007 **(0)**	0.001-0.011	<0.005-0.023 **(55)**	<0.005-2.65 **(43)**	14.8-16.5 **(100)**	0.16
PFHpS	<0.0009 **(0)**	<0.0009-0.002 **(10)**	<0.0009 **(0)**	<0.0009	<0.0009 **(0)**	0.0008-0.002	N.M	N.M	N.M	N.M
PFOS	<0.001-0.095 **(50)**	<0.001-0.13 **(90)**	<0.001-0.046 **(83)**	0.015	0.023-0.062 **(100)**	0.004-0.039	0.044-0.23 **(100)**	0.2-2.0 **(100)**	61.9-68.3 **(100)**	0.29
PFECHS	0.075-0.21 **(100)**	<0.001-0.89 **(80)**	<0.001 **(0)**	<0.001	<0.001 **(0)**	N.M	N.M	N.M	N.M	N.M
FOSA	<0.0002-0.023 **(50)**	<0.0002-0.009 **(50)**	<0.0002 **(0)**	<0.0002	<0.0002 **(0)**	<0.001	N.M	N.M	N.M	N.M
ΣPFAS	8.9-9.4	2.6-21	1.1-4.1	0.59	0.14-0.40	0.027-0.456	0.12-4.11	3.4-9.6	112-119	3.5

Table S6. Summary of LOADEST model statistics. Bias percentage (%): <0 = underestimation, >0 = overestimation; partial ratio (PLR): >1 = overestimation, <1 = underestimation; Nash Sutcliffe Efficiency Index (E): 1 = perfect fit, 0 = model estimate is equivalent to data mean, <0 = observed mean is better than model estimate.

	R^2	Bias	PLR	E
PFBA	97.17	-1.665	0.9833	0.977
PFHxA	97.93	0.7721	1.008	0.8787
PFHpA	97.22	-2.079	0.9792	0.5103
PFOA	97.58	0.7816	1.008	0.8144
PFNA	97.96	-1.38	0.9862	0.8162
ΣPFAS	97.57	-0.533	0.9947	0.959

Table S7. Summary of the mass transfer analysis in the Lake Hazen watershed during 2015. Glacial inputs (kg) are calculated as the sum of daily riverine fluxes during the 2015 glacier melting season from 1 June to 19 August. Fluxes are estimated using a LOADEST log-linear model. Uncertainty is represented by standard error. †Rivers sampled correspond to 84% of the watershed area. A factor of 1.19 was applied to scale the total glacial input to the entire watershed. Snowmelt inputs (kg) were calculated using average PFAS concentrations in 2013 snowpacks[10] from the ice surface of Lake Hazen and the snowmelt runoff volume in 2015 (0.127 km^3). The output (kg) by the Ruggles River was calculated using PFAS concentrations in its outflow and its annual output in 2015 (1.093 km^3). The net change (ΔPFAS, kg) is calculated as the difference between inputs by snowmelt and glacial rivers and the output by the Ruggles River. Only PFAS congeners with high detection frequencies in glacial rivers were chosen for this analysis. As only one sample was collected from the Ruggles River, the propagated uncertainty in ΔPFAS is reflective of uncertainties in the inputs from glacial rivers and snowmelt.

	Total Glacial Input†	Snowmelt	Output	ΔPFAS
PFBA	1.0 ± 0.47	0.19 ± 0.14	0.48	0.72 ± 0.49
PFHxA	0.079 ± 0.036	0.020 ± 0.017	0.017	0.082 ± 0.040
PFHpA	0.11 ± 0.061	0.056 ± 0.042	0.028	0.14 ± 0.074
PFOA	0.16 ± 0.087	0.063 ± 0.047	0.072	0.15 ± 0.099
PFNA	0.11 ± 0.061	0.071 ± 0.056	0.028	0.15 ± 0.083
ΣPFAS	1.6 ± 0.72	0.44 ± 0.32	0.64	1.4 ± 0.79

Table S8. Concentration ranges (ng L^{-1}) and detection frequencies (%) along the Skeleton Continuum during July-August 2015 and in snowpacks[10] from the Lake Hazen area in 2013 and 2014. Detection frequencies are calculated as the percent number of samples out of the sampling dates (*n*) with concentrations >LOD, and are presented in bold text in parentheses.

	Skeleton Continuum					**Lake Hazen Snowpacks**		
	S1	**S2**	**S3**	**S4**	**S5**	**Light (13')**	**Light (14')**	**Dark (14')**
PFBA	1.9-3.7 **(100)**	2.8-3.8 **(100)**	2.5-3.0 **(100)**	1.3-1.5 **(100)**	1.1-1.4 **(100)**	1.2-52 **(100)**	1.8-3.8 **(100)**	2.3-11 **(100)**
PFPeA	<0.010 **(0)**	<0.010 **(0)**	<0.010 **(0)**	<0.010 **(0)**	<0.010 **(0)**	0.097-1.6 **(100)**	0.083-0.21 **(100)**	0.18-1.5 **(100)**
PFHxA	0.11-0.18 **(100)**	0.17-0.23 **(100)**	0.14-0.24 **(100)**	<0.005-0.029 **(33)**	<0.005 **(0)**	0.12-1.3 **(100)**	0.16-0.38 **(100)**	0.36-1.6 **(100)**
PFHpA	0.060-0.094 **(100)**	0.12-0.17 **(100)**	0.075-0.13 **(100)**	<0.002 **(0)**	<0.002-0.044 **(33)**	0.38-4.3 **(100)**	0.29-0.70 **(100)**	0.54-2.9 **(100)**
PFOA	0.074-0.10 **(100)**	0.094-0.15 **(100)**	0.069-0.13 **(100)**	0.025-0.039 **(100)**	0.034-0.047 **(100)**	0.35-10 **(100)**	0.46-1.1 **(100)**	0.92-4.9 **(100)**
PFNA	<0.002-0.004 **(20)**	0.017-0.061 **(100)**	<0.002-0.038 **(66)**	<0.002 **(0)**	<0.002-0.014 **(66)**	0.39-3.1 **(100)**	0.37-0.94 **(100)**	0.76-5.3 **(100)**
PFDA	<0.003-0.003 **(40)**	<0.003-0.007 **(20)**	<0.003-0.005 **(33)**	<0.003 **(0)**	<0.003-0.032 **(33)**	0.082-0.56 **(100)**	0.086-0.24 **(100)**	0.16-1.7 **(100)**
PFUnDA	<0.003 **(0)**	<0.003 **(0)**	<0.003 **(0)**	<0.003 **(0)**	<0.003 **(0)**	0.048-0.17 **(100)**	0.052-0.17 **(100)**	0.088-0.80 **(100)**
PFDoDA	<0.002 **(0)**	<0.002 **(0)**	<0.002 **(0)**	<0.002 **(0)**	<0.002 **(0)**	0.012-0.051 **(100)**	0.010-0.12 **(100)**	0.020-0.31 **(100)**
PFTrDA	<0.002 **(0)**	<0.002-0.004 **(20)**	<0.002 **(0)**	<0.002 **(0)**	<0.002 **(0)**	<0.002 **(0)**	<0.002-0.010 **(33)**	<0.002-0.10 **(89)**
PFTeDA	<0.003-0.003 **(20)**	<0.003-0.004 **(20)**	<0.003 **(0)**	<0.003 **(0)**	<0.003 **(0)**	<0.003-0.023 **(75)**	<0.003-0.007 **(22)**	<0.003-0.019 **(44)**
PFHxDA	<0.010 **(0)**	<0.010 **(0)**	<0.010 **(0)**	<0.010 **(0)**	<0.010 **(0)**	<0.010 **(0)**	<0.010 **(0)**	<0.010 **(0)**
PFBS	0.36-0.41 **(100)**	0.25-0.26 **(100)**	0.30-0.31 **(100)**	0.21-0.25 **(100)**	0.18-0.24 **(100)**	<0.002-0.40 **(25)**	<0.002-0.011 **(44)**	<0.003-0.024 **(78)**
PFHxS	0.037-0.051 **(100)**	<0.0007 **(0)**	<0.0007 **(0)**	<0.0007-0.014 **(33)**	<0.0007 **(0)**	<0.001-0.44 **(25)**	<0.0007 **(0)**	<0.001-0.004 **(11)**
PFHpS	<0.0009 **(0)**	0.097-0.12 **(100)**	0.045-0.060 **(100)**	<0.0009-0.054 **(33)**	0.038-0.044 **(100)**	<0.0009 **(0)**	<0.0009 **(0)**	<0.0009 **(0)**
PFOS	<0.001-0.047 **(60)**	0.013-0.020 **(100)**	<0.001-0.019 **(66)**	<0.001-0.21 **(33)**	<0.001-0.017 **(33)**	0.009-1.0 **(100)**	0.009-0.051 **(100)**	0.035-0.44 **(100)**
PFECHS	<0.001-0.001 **(20)**	<0.001-0.002 **(20)**	<0.001 **(0)**	<0.001 **(0)**	<0.001 **(0)**	<0.001-0.059 **(87)**	<0.001-0.022 **(55)**	<0.001-0.009 **(44)**
PFDS	<0.0006 **(0)**	<0.0006 **(0)**	<0.0006 **(0)**	<0.0006 **(0)**	<0.0006 **(0)**	<0.0006 **(0)**	<0.0006 **(0)**	<0.0006 **(0)**
FOSA	<0.0002 **(0)**	<0.0002-0.029 **(20)**	<0.0002 **(0)**	<0.0002 **(0)**	<0.0002 **(0)**	<0.0002 **(0)**	<0.0002 **(0)**	<0.0002 **(0)**

Table S9. Spearman correlation (r_s) analysis of PFAA concentrations along the Skeleton Continuum during July 2015. Correlation analysis was limited to PFAA with detection frequencies equal to or greater than 50%. Statistically significant correlations ($p<0.05$) are bolded.

		PFBA	**PFHxA**	**PFHpA**	**PFOA**	**PFNA**	**PFBS**	**PFHpS**
PFHxA	r_s	0.33						
	p	0.25						
PFHpA	r_s	0.50	**0.73**					
	p	0.07	**<0.01**					
PFOA	r_s	**0.77**	0.49	**0.78**				
	p	**<0.01**	0.08	**<0.01**				
PFNA	r_s	0.36	0.33	**0.76**	0.62			
	p	0.31	0.42	**0.02**	0.06			
PFBS	r_s	**0.60**	-0.31	-0.35	**0.48**	0.25		
	p	**<0.01**	0.28	0.22	**0.04**	0.48		
PFHpS	r_s	**0.80**	0.02	**0.75**	**0.77**	0.63	0.39	
	p	**<0.01**	0.97	**0.02**	**<0.01**	0.07	0.21	
PFOS	r_s	-0.27	-0.16	0.23	0.02	0.05	-0.12	-0.07
	p	0.40	0.64	0.50	0.95	0.91	0.69	0.86

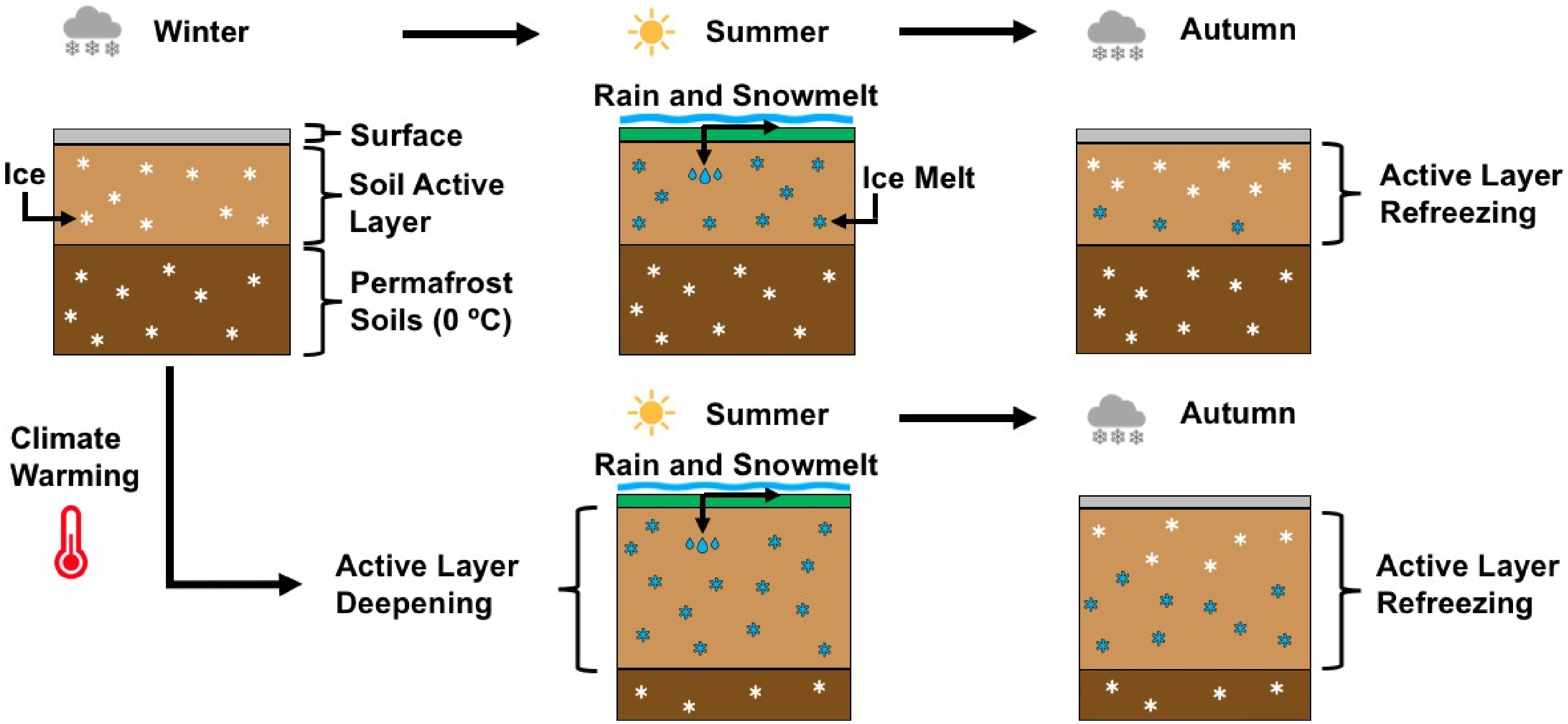

Figure S1. Schematic of seasonal ice melt and permafrost degradation in Arctic soils. During the summer, Arctic soils thaw and ice contained in those soils melts. The soil active layer receives inputs from atmospheric precipitation, snowmelt, and ice contained in active layer/permafrost soils, which can be discharge to freshwater ecosystems.

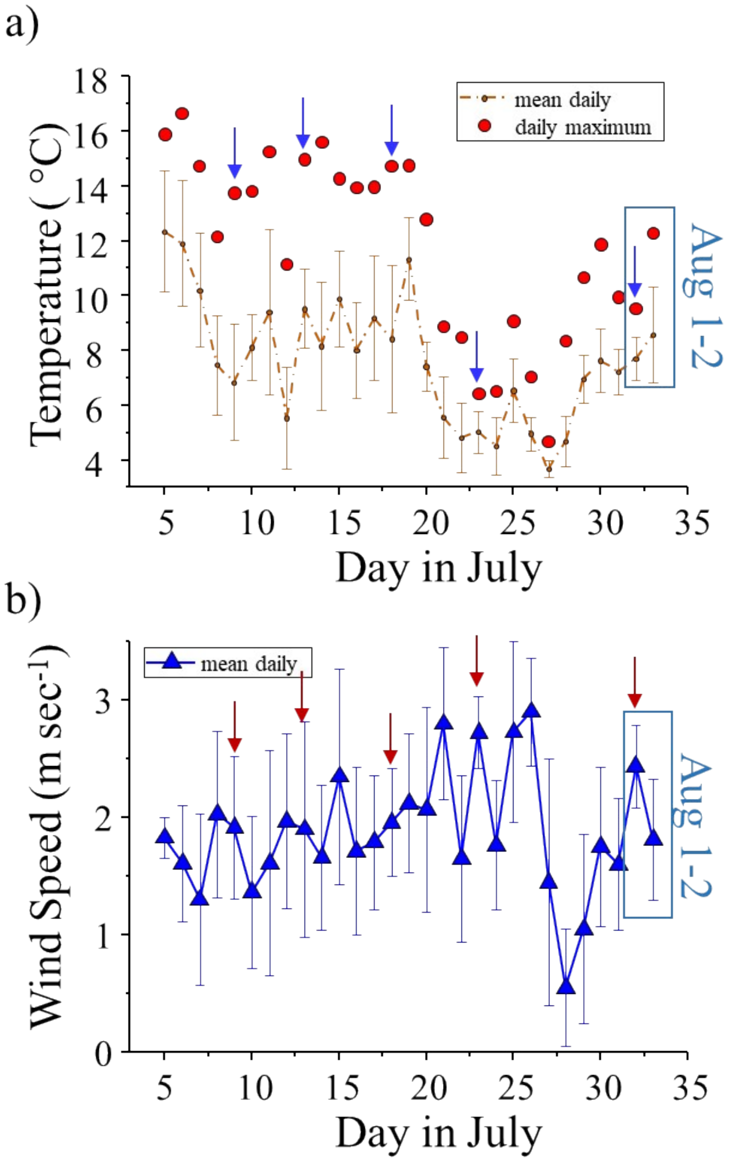

Figure S2. Meteorological conditions at Lake Hazen: a) mean ± standard deviation daily temperature and maximum daily temperature and b) mean ± standard deviation daily wind speed, based on hourly recording from 5 July to 2 August 2015 using a portable weather station (Campbell Scientific). Arrows indicate sampling points.

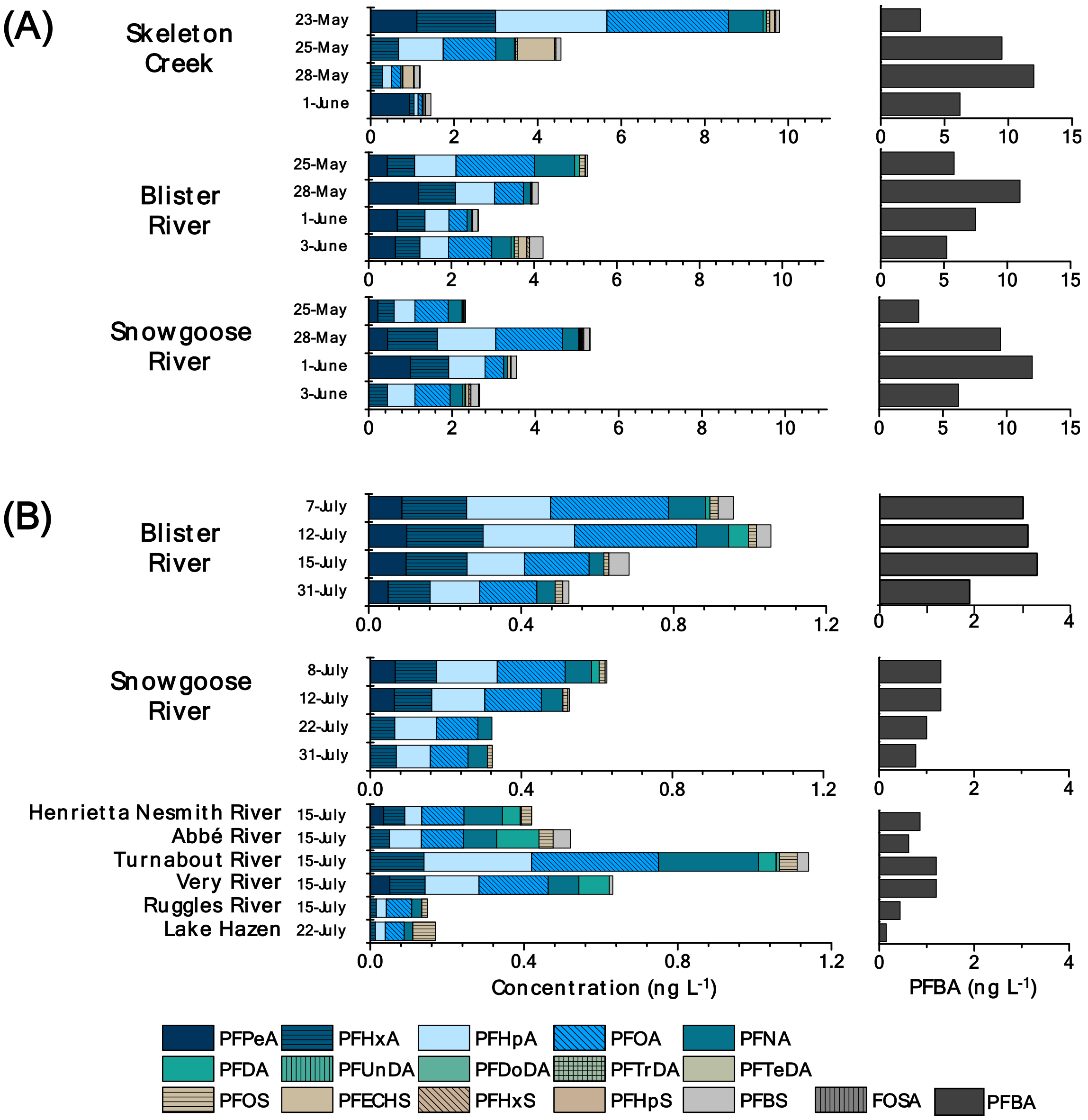

Figure S3. PFAS concentrations (ng L^{-1}) in river, creek, and lake water from the Lake Hazen watershed during snowmelt from 23 May to 1 June 2014 and 3 June 2012 (panel A) and during glacial ice melting from 7 to 31 July 2015 (panel B). Surface water from Lake Hazen (0 m depth) is shown for comparison in panel B. Note the different scales in panels A and B.

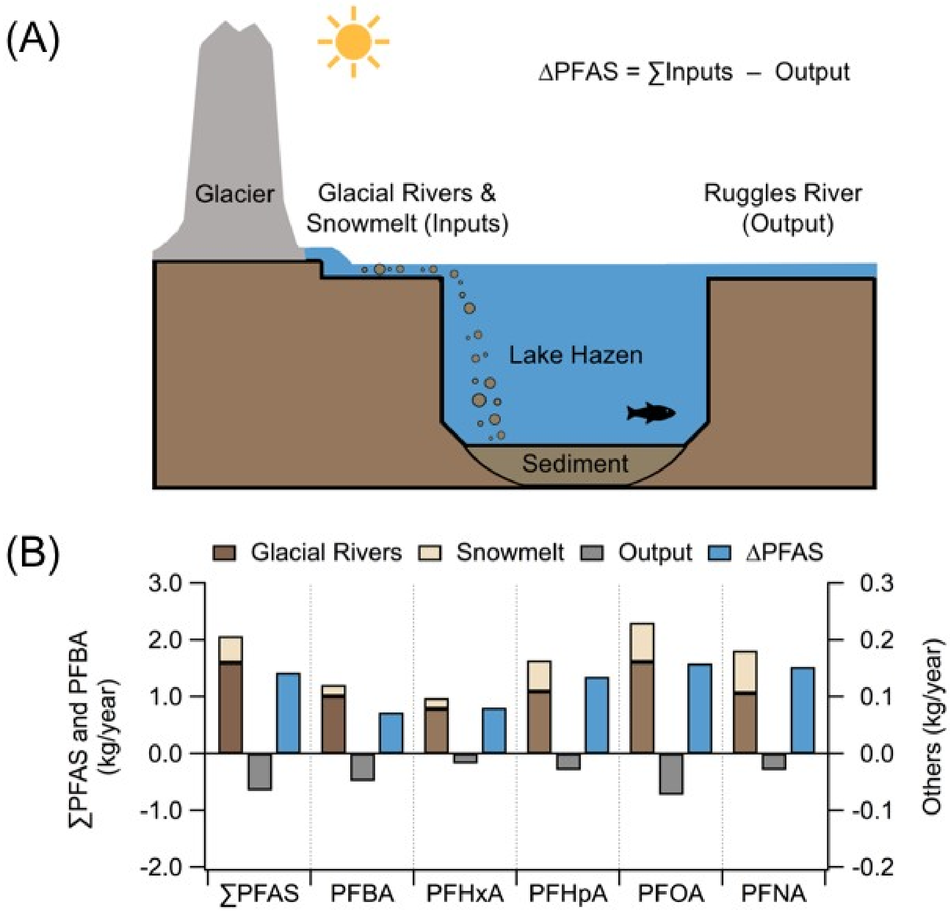

Figure S4. (A) Schematic of inputs and outputs in the Lake Hazen watershed. (B) Mass transfer analysis for ΣPFAS (left axis) and select PFAS congeners (right axis) in the Lake Hazen watershed.

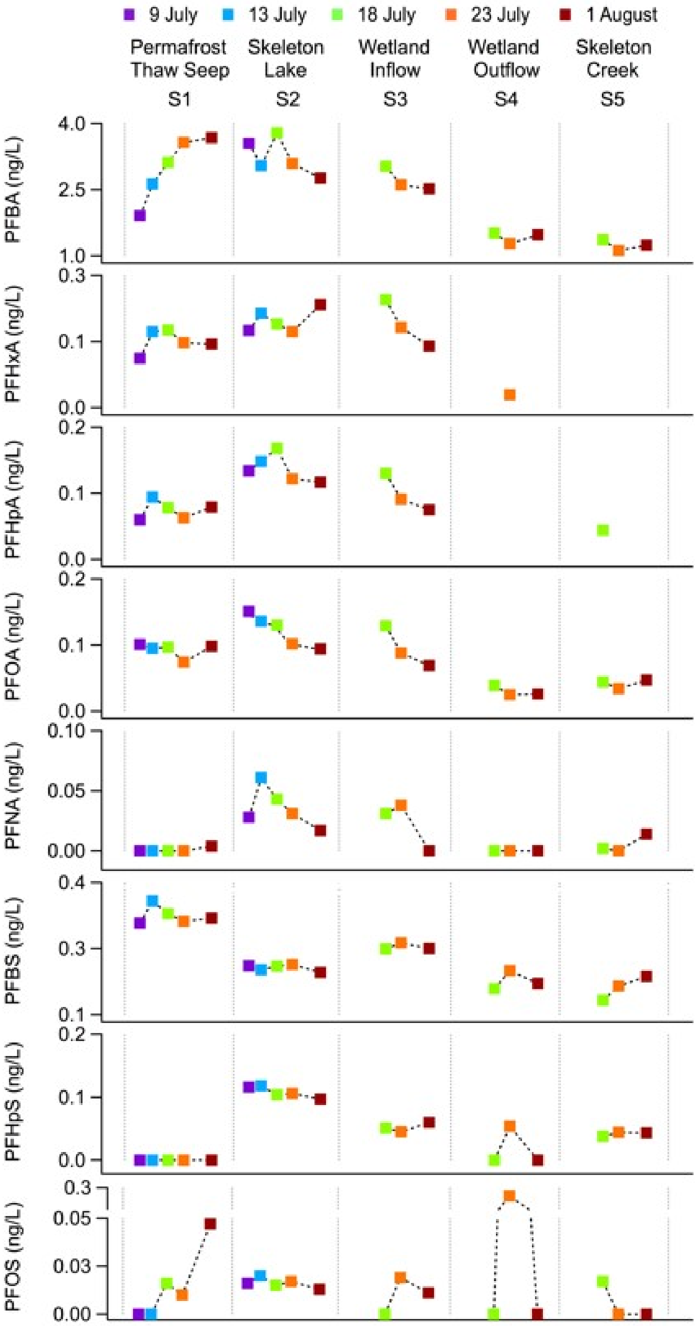

Figure S5. PFAS concentrations (ng L^{-1}) along the Skeleton Continuum from 9 July to 1 August 2015. Note sampling was not conducted on 9 and 13 July at S3-S5 because water was not flowing through those sites during those periods. Only congeners with high detection frequencies are included in this figure (see Table S8).

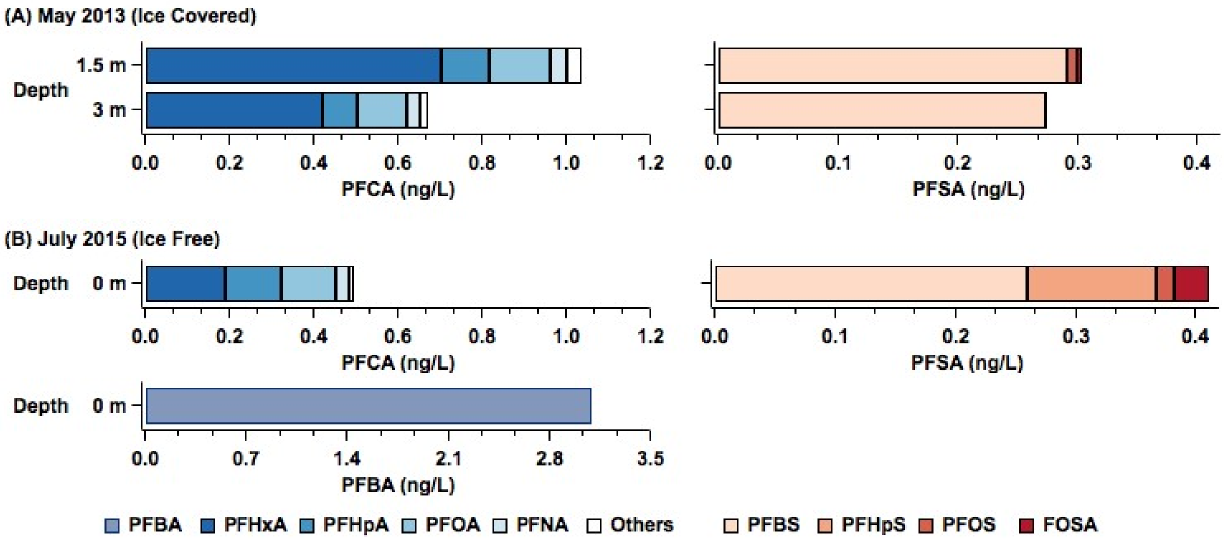

Figure S6. PFAS concentrations (ng L^{-1}) in Skeleton Lake (S2) during an ice-covered period in May 2013 (1.5 and 3 m depths) and during an ice-free period in July 2015 (0 m depth). A median PFAS concentration is shown in S2 during the ice-free period from 9 July to 1 August 2015. The ice-covered period in May 2013 is representative of melting inputs from the previous summer because the surface of S2 freezes over beginning in September, preserving hydrological inputs under the ice until the following spring. Others corresponds to the sum of C_{10}-C_{14} PFCA. PFECHS was detected in S2 in 2015 (Table S8) but is not included in this figure due to its low concentration.

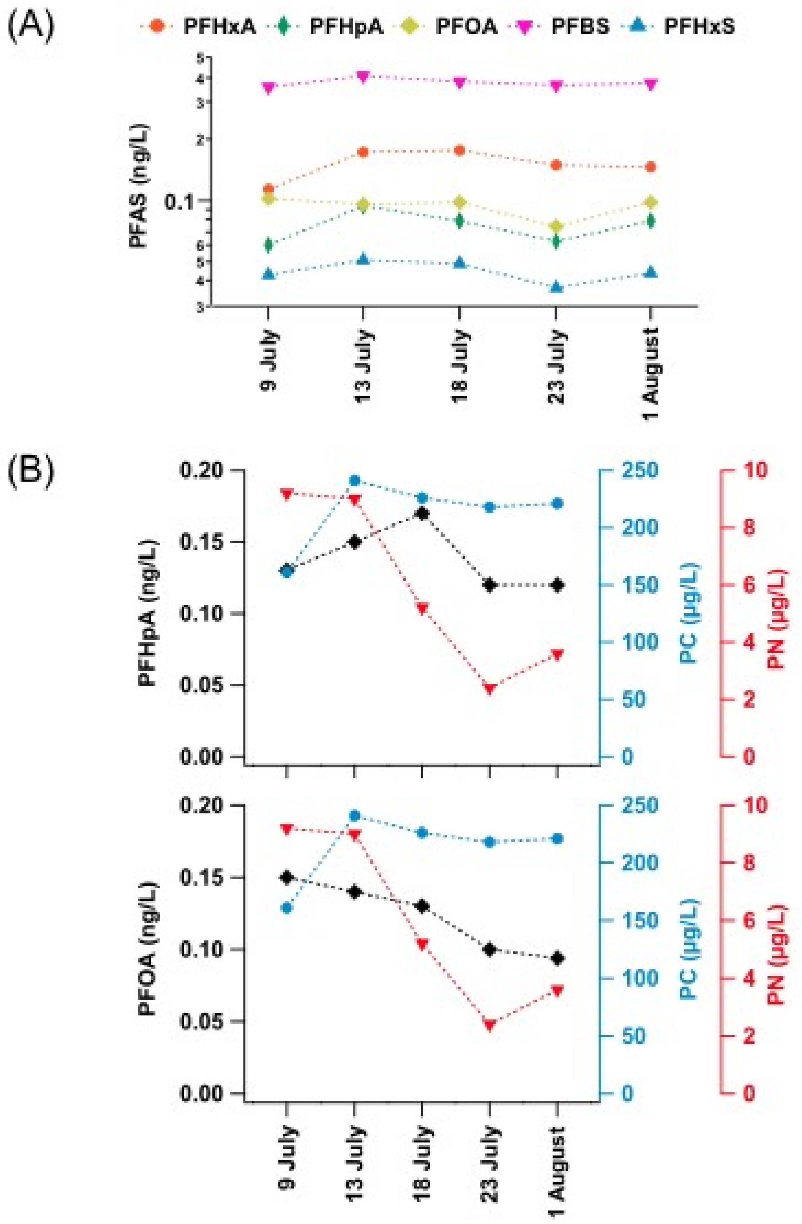

Figure S7. PFAS concentrations at the permafrost thaw seep (S1, panel A) and PFHpA, PFOA (ng L^{-1}, black squares, left y-axis), particulate carbon (PC, blue circles and right y-axis), and nitrogen (PN, red triangles and right y-axis) concentrations (µg L^{-1}) in Skeleton Lake (S2, panel B) during 9 July to 1 August 2015.

References

1 M. K. Woo, *Permafrost hydrology*, Springer, Heidelberg, 2012.

2 K. A. St. Pierre, V. L. St. Louis, I. Lehnherr, A. S. Gardner, J. A. Serbu, C. A. Mortimer, D. C. G. Muir, J. A. Wiklund, D. Lemire, L. Szostek and C. Talbot, Drivers of mercury cycling in the rapidly changing glacierized watershed of the High Arctic's largest lake by Volume (Lake Hazen, Nunavut, Canada), *Environ. Sci. Technol.*, 2019, **53**, 1175–1185.

3 I. Lehnherr, V. L. St. Louis and J. L. Kirk, Methylmercury cycling in high arctic wetland ponds: Controls on sedimentary production, *Environ. Sci. Technol.*, 2012, **46**, 10523–10531.

4 C. A. Emmerton, V. L. St. Louis, E. R. Humphreys, J. A. Gamon, J. D. Barker and G. Z. Pastorello, Net ecosystem exchange of CO_2 with rapidly changing high Arctic landscapes, *Glob. Chang. Biol.*, 2016, **22**, 1185–1200.

5 R. N. Sinnatamby, J. A. Babaluk, G. Power, J. D. Reist and M. Power, Summer habitat use and feeding of juvenile Arctic charr, Salvelinus alpinus, in the Canadian High Arctic, *Ecol. Freshw. Fish*, 2012, **21**, 309-322.

6 A. O. De Silva, C. Spencer, B. F. Scott, S. Backus and D. C. G. Muir, Detection of a cyclic perfluorinated acid, perfluoroethylcyclohexane sulfonate, in the great lakes of North America, *Environ. Sci. Technol.*, 2011, **45**, 8060–8066.

7 G. L. Lescord, K. A. Kidd, A. O. De Silva, M. Williamson, C. Spencer, X. Wang and D. C. G. Muir, Perfluorinated and polyfluorinated compounds in lake food webs from the Canadian High Arctic, *Environ. Sci. Technol.*, 2015, **49**, 2694–2702.

8 J. J. MacInnis, K. French, D. C. G. Muir, C. Spencer, A. Criscitiello, A. O. De Silva and C. J. Young, Emerging investigator series: a 14-year depositional ice record of perfluoroalkyl substances in the High Arctic, *Environ. Sci. Process. Impacts*, 2017, **19**, 22–30.

9 H. M. Pickard, A. Criscitiello, C. Spencer, M. J. Sharp, D. C. G. Muir, A. O. De Silva and C. J. Young, Continuous non-marine inputs of per- and polyfluoroalkyl substances to the high Arctic: A multi-decadal temporal record, *Atmos. Chem. Phys.*, 2018, **18**, 5045–5058.

10 J. J. MacInnis, I. Lehnherr, D. C. G. Muir, K. A. St. Pierre, V. L. St. Louis, C. Spencer and A. O. De Silva, Fate and transport of perfluoroalkyl substances from snowpacks into a lake in the High Arctic of Canada, *Environ. Sci. Technol.*, 2019, **53**, 10753–10762.

11 J. J. MacInnis, I. Lehnherr, D. C. G. Muir, R. Quinlan and A. O. De Silva, Characterization of perfluoroalkyl substances in sediment cores from High and Low Arctic lakes in Canada, *Sci. Total Environ.*, 2019, **666**, 414–422.

12 D. Lorenz, R. Runkel and L. De Cicco, rloadest: river load estimation; U.S. Geological Survey: Mounds View, Minnesota, USA, 2015.

13 K.-U. Goss, The pKa values of PFOA and other highly fluorinated carboxylic acids, *Environ. Sci. Technol.,* 2008, **42**, 456–458.

14 J. Veillette, D. Muir, D. Antoniades, J. M. Small, C. Spencer, T. N. Loewen, J. A. Babaluk, J. D. Reist and W. F. Vincent, Perfluorinated chemicals in meromictic lakes on the northern coast of Ellesmere Island, High Arctic Canada, *Arctic*, 2012, **65**, 245–256.

15 J. S. Skaar, E. M. Ræder, J. L. Lyche, L. Ahrens and R. Kallenborn, Elucidation of contamination sources for poly- and perfluoroalkyl substances (PFASs) on Svalbard (Norwegian Arctic), *Environ. Sci. Pollut. Res.*, 2019, **26**, 7356–7363.

16 K. Y. Kwok, E. Yamazaki, N. Yamashita, S. Taniyasu, M. B. Murphy, Y. Horii, G. Petrick, R. Kallenborn, K. Kannan, K. Murano, and P. K. S. Lam, Transport of perfluoroalkyl substances (PFAS) from an arctic glacier to downstream locations: Implications for sources, *Sci. Total Environ.*, 2013, **447**, 46–55.